Retrospective correction of involuntary microscopic head-movement using highly-accelerated fat image-navigators (3D FatNavs) at 7T

Daniel Gallichan[1], José P Marques[2], Rolf Gruetter[1,2,3]

[1]CIBM, EPFL Lausanne, Switzerland, [2]Dept. of Radiology, University of Lausanne, Switzerland,
[3]Dept. of Radiology, University of Geneva, Switzerland

Abstract

Purpose

The aim of the present study was to use a 3D gradient-echo volume in combination with a fat-selective excitation as a 3D motion navigator (3D FatNav) for retrospective correction of microscopic head-motion during high-resolution 3D structural scans of extended duration. The fat excitation leads to a 3D image which is itself sparse, allowing high parallel imaging acceleration factors – with the additional advantage of a minimal disturbance of the water signal used for the host sequence.

Methods

A 3D FatNav was inserted into two structural protocols – an inversion-prepared gradient-echo at 0.33×0.33×1.00 mm resolution and a turbo spin-echo at 600 μm isotropic resolution.

Results

Motion estimation was possible with high-precision, allowing retrospective motion-correction to give clear improvements in image quality, especially in the conspicuity of very small blood vessels.

Conclusion

The highly accelerated 3D FatNav allowed motion-correction with noticeable improvements in image quality, even for head-motion which was small compared to the voxel dimensions of the host sequence.

Introduction

Recent technological developments in both hardware and software have lead to substantially increased spatial resolution in MRI. As resolution improves, the image quality is increasingly sensitive to small involuntary motion of the subject. Various motion-correction methods have been proposed, including techniques using external markers for a tracking system (1–5) or MR-navigator based methods which can either use data directly from the imaging sequence itself (6,7) or interleave a rapid navigator within the host sequence (8–11). The majority of existing methods have concentrated on the correction of moderate to large scale motion of the subject (i.e. > ~5 mm translation and > ~5° rotation), with healthy volunteers being asked to make deliberate movements in order to test the correction methods. Recent work has also demonstrated the utility of the detection and correction of the microscopic motion of compliant subjects (root-mean square ≤ ~2mm translation and ≤ ~2° rotation) that is unavoidable for durations required for imaging at very high spatial resolution (3,5,12). An external camera/marker system was used to achieve these results – for which the spatial constraints of the MR system and RF head coil can cause installation difficulties. Modern MR systems often have RF arrays for neuroimaging with 32 receive channels or more, with close-fitting designs which leave little room to establish line-of-sight between a bore-mounted camera and marker(s) attached to the subject's head. An existing approach compatible with most RF coil designs is to mount the marker on a dental-fit mouthpiece (5,12), but this needs to be fabricated for each subject – limiting how readily the method may be applied for routine use.

A recent preliminary study demonstrated that very high resolution images (350 μm isotropic) could be achieved at 3T using a 138-minute protocol interleaved with volumetric echo-planar imaging (EPI)-based navigators (vNavs) (13). It is unclear, however, what the expected precision of the vNavs should be in their current implementation (8mm isotropic resolution multi-shot EPI) – and it would be expected that this performance will diminish at 7T due to the increased image distortions and signal dropouts due to increased B_0 variations at higher field.

It has previously been demonstrated that a fat-selective RF pulse can be useful as a motion-navigator for cardiac applications (14) and some tests have also been performed for head imaging (15). Therefore the aim of the present study was to demonstrate the feasibility of a navigator-based correction method at 7T suitable for high-resolution imaging with no deliberate motion of the subject and requiring a negligible increase in scan time, exploiting the natural sparsity of fat-only head images (as the signal is primarily localized to sub-cutaneous fat and bone-marrow in the skull) to allow a highly accelerated parallel acquisition. It was noted in other recent work on fat-based navigators (16) that acceleration factors of up to 8 could be used for a 2D fat-image with only minor image degradation, using a conventional GRAPPA (Generalized autocalibrating partially parallel acquisitions (17)) method for image reconstruction on data acquired with an 8-channel RF coil. In our study, using a 32-channel coil and a 3D acquisition, we expect to be able to achieve considerably higher acceleration than 8. Initial results of our method applied in vivo have recently been presented in abstract form (18).
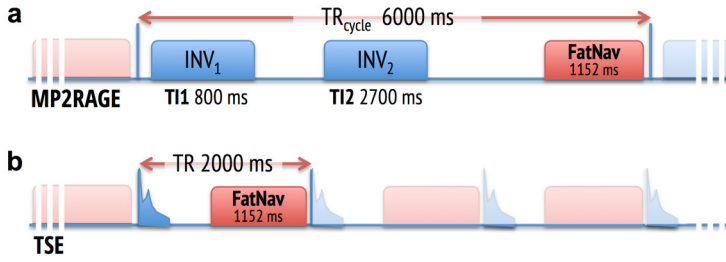
Fig. 1. Pulse sequence diagrams of (a) the MP2RAGE sequence and (b) the TSE sequence as used in Experiments 3 and 4 of this study, showing the relative timing of the 1152 ms 3D FatNav with 2 mm isotropic resolution, with an acceleration of 4×4=16.

Methods

All imaging was performed on a 7T head-only MR system (Siemens Healthcare, Erlangen, Germany) fitted with a 32-channel RF coil array, housed within a birdcage transmit coil (Nova Medical Inc., Wilmington, MA). All volunteers were young healthy adults (19-35 years) who gave written informed consent prior to the imaging in accordance with the local review board.

The highly accelerated fat motion-navigators (3D FatNavs)
With the aim of correcting for microscopic level motion, we chose an isotropic resolution for the 3D FatNavs of 2 mm, with the hope of being able to precisely detect motion approaching a similar level as that having been reported due to the ballistocardiogram of ~140 μm (5) – motion which occurs very quickly during the cardiac-cycle, and represents an upper limit on the useful resolution of a navigator which will not be fast enough to track this small motion. A 3D-GRE acquisition was used with a 3-pulse binomial excitation pulse to selectively excite at the frequency of fat (~1000 Hz from water at 7T) with a 88×128×128 matrix, TE/TR=1.35/3.0 ms, bandwidth = 1950 Hz/Px, flip angle 7°, readout direction foot/head. Partial-Fourier undersampling (reconstructed with zero-filling) was used for all FatNavs to reduce the TR_{volume} by 44% at the expense of a small loss of effective resolution. A fully-sampled acquisition with these parameters requires 19.0 s.

Experiment 1: Evaluation of achievable GRAPPA acceleration for 3D FatNavs
Two fully-sampled volumes were acquired with the parameters described above. After a Fourier transform in the readout direction, a single transverse slice of data was selected as an example for testing acceleration factors. The central 20×32 samples from the first volume were used for the calibration of the GRAPPA weights. The data from the second volume were decimated to simulate various acceleration factors (2 to 10 per phase-encoding direction, corresponding to total acceleration of 4 to 100 times), and then reconstructed using a GRAPPA kernel with 2×2 source points at each acceleration factor. The same process was repeated with a non-selective excitation to compare the reconstruction quality at each acceleration factor with a conventional water-image.

Experiment 2: High-resolution MP2RAGE scan motion-corrected with 3D FatNavs
An acceleration factor of 4×4=16 was chosen for the 3D FatNav used to correct the structural data, as the results

of Experiment 1 indicated a good image quality at this acceleration factor, and the navigator duration of 1.15 s can be inserted into existing high-resolution protocols for MP2RAGE (*Magnetization Prepared 2 Rapid Acquisition Gradient Echoes* (19)) acquisitions without additional scan time as there is already sufficient 'dead-time' between inversion pulses waiting for signal recovery. The binomial pulse used for fat excitation has a low flip angle (7°) for fat, and is therefore expected to have a negligible effect on the water signal recovery, despite 384 excitations during the 1.15 s.

For the MP2RAGE scan, a nominal resolution of 0.33×0.33×1.00 mm was used (488×492×80 matrix, FoV 160×160×80 mm, 6/8 partial Fourier) resulting in coverage of most of the brain. $TE/TI_1/TI_2/TR$ = 6.06/800/2700/6000 ms, bandwidth = 280 Hz/Px, flip angle (TI_1/TI_2) = 7°/5°, readout direction anterior/posterior, phase-encoding direction right/left, with flow compensation in the partition-encoding direction. The total scan time for the MP2RAGE scan was 36m 38s and an additional 2.3s was added to the start of the scan to acquire 20×32 lines of fully-sampled fat-excitation data from which to determine the GRAPPA weights for the 3D FatNavs, using a 2×2 kernel. Figure 1a shows a diagram of one TR of the pulse sequence, and the relative timing of the 3D FatNav.

All raw data were processed using Matlab (the Mathworks Inc, Natick, MA), firstly reconstructing each of the 366 3D FatNavs, then performing rigid-body co-registration of each 3D FatNav to the first using a least-squares cost function with the *realign* tool in SPM (*Statistical Parametric Mapping, version 8*) using the highest 'quality' setting (1.0) and with the other parameters left at their default settings (5 mm FWHM Gaussian smoothing prior to realignment, degree 2 B-spline interpolation, 4 mm separation of image samples). Estimated motion parameters were subsequently recentered such that 'zero motion' was defined as the time coincident with the acquisition of the center of k-space (1/3 of the total scan time due to use of partial Fourier) in order to maintain the strongest visual similarity between reconstructed images before and after motion-correction. Retrospective motion correction of the MP2RAGE data was performed in k-space by using the motion parameters from the 3D FatNav acquired closest in time (effectively applying one set of motion-parameters per k-space plane in the partition-encoding direction), with translations corresponding to simple phase ramps, and rotations requiring 3D regridding, which was performed using the 3D Non-Uniform Fast
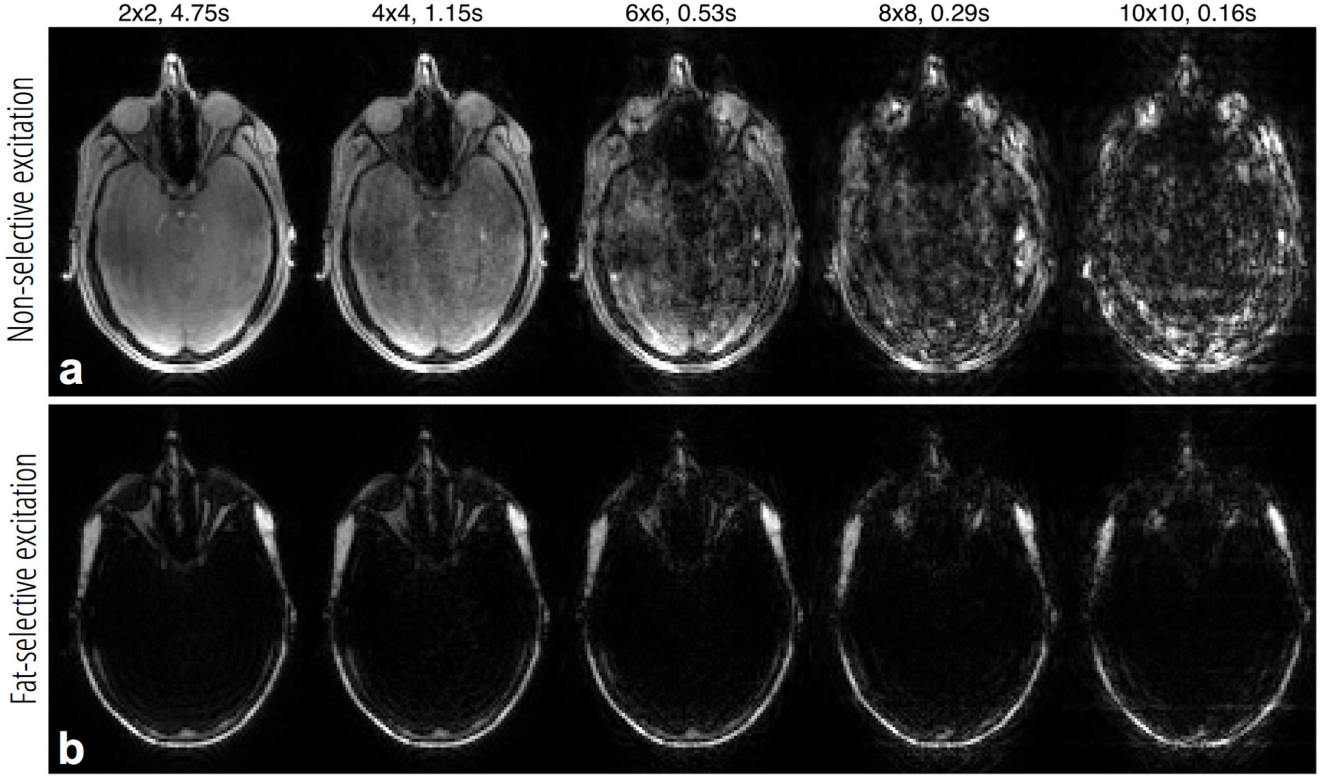
2

Figure 2. A single slice of a 3D GRE acquisition of the whole head using (a) non-selective excitation and (b) fat-excitation. The data were retrospectively undersampled by increasing acceleration factors (2×2 through to 10×10, with corresponding TR_{volume} also shown) and reconstructed using GRAPPA weights determined from separate calibration data.

Fourier Transform (NUFFT) algorithm (20) provided by Jeffrey Fessler's reconstruction toolbox (http://web.eecs.umich.edu/~fessler/code/). Assuming small motion, no density compensation was applied to compensate for the changes in k-space sample density resulting from the rotations. All corrections were performed separately for the data from each RF channel prior to calculating the MP2RAGE image by combination of the complex images from each inversion time:

$$MP2RAGE_\alpha = real\left(\frac{GRE^*_{TI1,\alpha}GRE_{TI2,\alpha}}{\left|GRE_{TI1,\alpha}\right|^2+\left|GRE_{TI2,\alpha}\right|^2}\right)$$

where $GRE_{TI1,\alpha}$ is the image generated from the data acquired at the first inversion time (TI1) for the coil channel index α, and the asterisk denotes complex conjugation. The final MP2RAGE image was combined from each coil channel as a weighted sum, where the weight was determined by $\left|GRE_{TI2,\alpha}\right|^2/\sum_i\left|GRE_{TI2,i}\right|^2$ for each voxel in each coil. The (unoptimized) regridding process took approximately 5 minutes per volume per RF channel on a Linux server with a 2×8-core 2.66 GHz CPUs and 96 Gb of RAM.

It has previously been noted that inversion-prepared GRE sequences can also be used for vessel visualization (21). The coil-combined image from the second inversion time, GRE_{TI2}, which was used to demonstrate vessel contrast, was produced by a root sum-of-squares from the separate coil images. The resulting GRE_{TI2} image was then processed using FAST software (FMRIB's Automated Segmentation Tool (22), part of the FMRIB Software Library, v5.0) to allow 'bias-field' correction to reduce the signal intensity variations across the brain due to the spatially varying sensitivity of the RF array. A projection of the maximum intensity over a thick slab allows visualization of arteries, and a minimum intensity projection allows visualization of veins.

Experiment 3: High resolution TSE scan motion-corrected with 3D FatNavs

For the turbo-spin-echo (TSE) sequence, a different volunteer was scanned with nominal isotropic resolution of 600 μm was used (384×384×288 matrix size, FoV 230×230×172.8 mm, 6/8 partial Fourier in the partition-encoding direction. TE/TR = 119/2000 ms, bandwidth = 543 Hx/Px, turbo factor 110, echo train duration 362 ms, readout direction foot/head, phase-encoding direction anterior/posterior, variable flip-angle train using vendor-supplied implementation based on the scheme described in ref (23). The total scan time was 33m 56s, with an additional 2.3 s for the GRAPPA calibration data for the 3D FatNavs. Figure 1b shows the relative timing of the pulse sequence and the inclusion of the 3D FatNav.

Experiment 4: Detection of head-motion due to the respiratory cycle with FatNavs

It has previously been demonstrated with external motion-tracking hardware that there is typically a small head-motion associated with the cardiac and respiratory cycles while a subject is lying supine within the MR system, predominantly along the z-axis (3,5). As preliminary experiments suggested that the precision of motion-estimation using the current parameters for the 3D FatNavs should be sufficient to detect motion on this order (~<100 μm amplitude fluctuations), we performed an additional experiment to test this – and to provide validation of the precision of the estimated motion
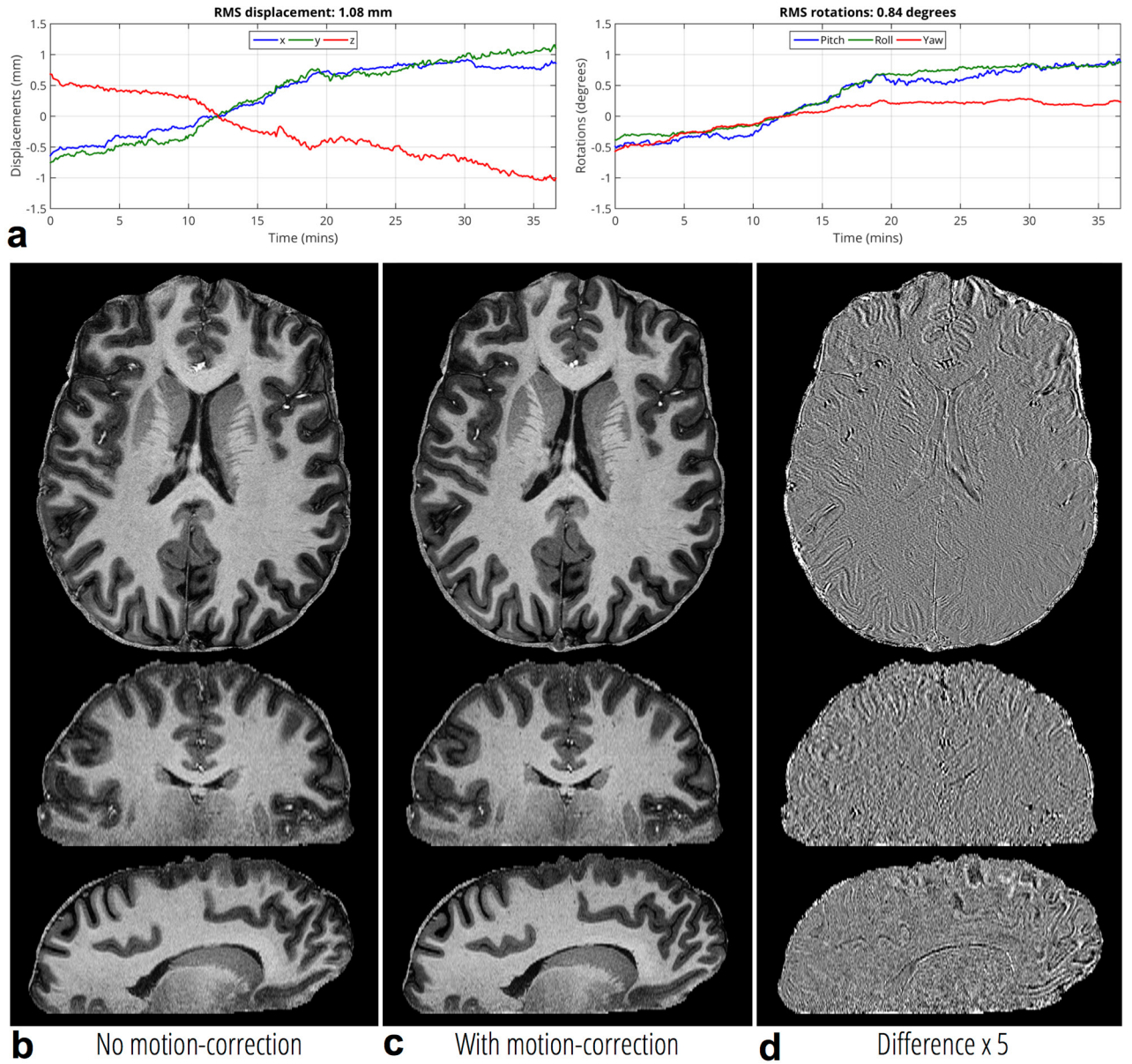
Figure 3. (a) Estimated rigid-body motion parameters obtained from 3D FatNavs (2mm, 4×4 acceleration) during ~37 minute MP2RAGE scan, 0.33×0.33×1.00 mm resolution (Experiment 2). (b) The high-resolution MP2RAGE volume. (c) The same MP2RAGE volume following retrospective motion-correction based on the estimated motion from the FatNavs. (d) The difference between the images before and after motion-correction.

parameters by showing that their fluctuations correspond to real subject motion even at very high resolution. For this experiment we needed a shorter TR$_{volume}$ to be able to reliably sample the respiration cycle so we used a 3D FatNav with 4 mm resolution and 4×4=16 acceleration, resulting in TR$_{volume}$ = 230 ms. Experiments 2 and 3 used a sampling rate for the FatNavs of 6 seconds and 2 seconds respectively (the TR of the respective sequences), which is also too long to reliably sample the respiratory cycle. Typical respiration cycles, however, should be adequately sampled by a volume TR of 230 ms.

A scan consisting only of 450 3D FatNavs was acquired, covering ~2 minutes with simultaneous logging of the data from the respiratory belt supplied with scanner for physiological monitoring. Processing to obtain motion-estimates from the FatNavs was identical to the previous experiments. For easier visual comparison of the respiratory trace with the z-component of the motion-

estimates, the estimated z-motion values were high-pass filtered to remove low-frequency drifts.

Results

Experiment 1: Evaluation of achievable GRAPPA acceleration for 3D FatNavs

Figure 2 compares reconstructions for of a single slice out of a fully-sampled 3D-GRE acquisition after retrospective decimation to simulate acquisitions at increasing 2D acceleration factors, following reconstruction using GRAPPA. The reconstructions from non-selective excitation data (Fig. 2a) exhibit small but noticeable artifacts at 4×4 acceleration, which become very strong when the acceleration reaches 6×6. For the reconstructions from the fat-excitation data there is only very minor deterioration of image quality up to acceleration of 6×6=36, but at 10×10=100 the edges start
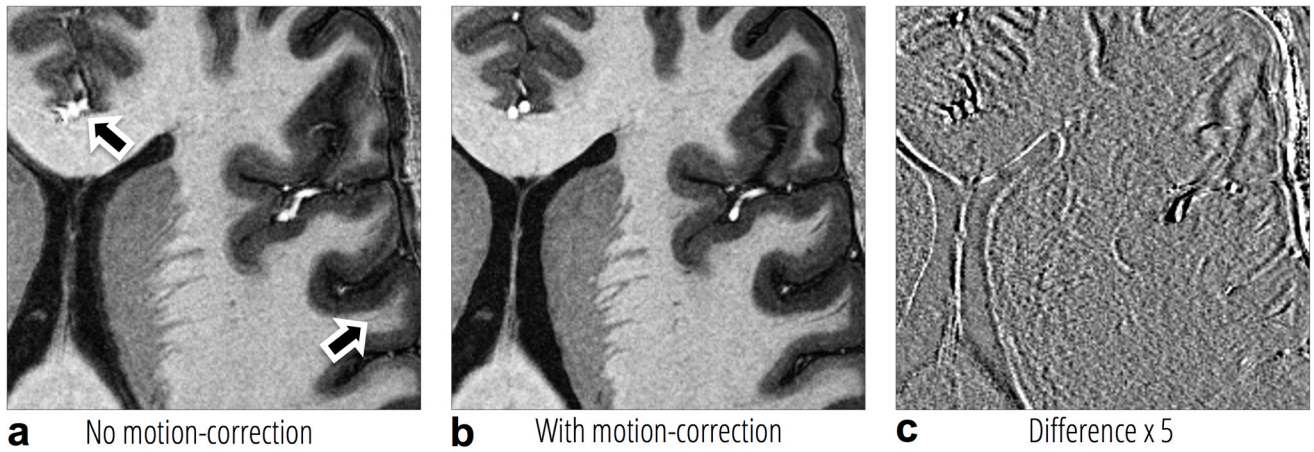
Figure 4. (a) Zoom of the same MP2RAGE dataset as shown in Fig. 3. (b) The same section following retrospective motion-correction. (c) The difference between the two. The arrows in (a) indicate regions where the improvement is most prominent. The overall improvement is best appreciated from the animated version of this figure, viewable online as Supporting Video S1.

Figure 5. (a) A zoomed section of the GRE_{TI2} volume from the same MP2RAGE dataset as shown in Figs. 3 and 4, with a minimum intensity projection taken over a 10 mm slab in the z-direction. (b) The same section following retrospective motion-correction. (c) The difference between the two. The arrows in (a) indicate regions where the improvement is most prominent. The overall improvement is best appreciated from the animated version of this figure, viewable online as Supporting Video S2.
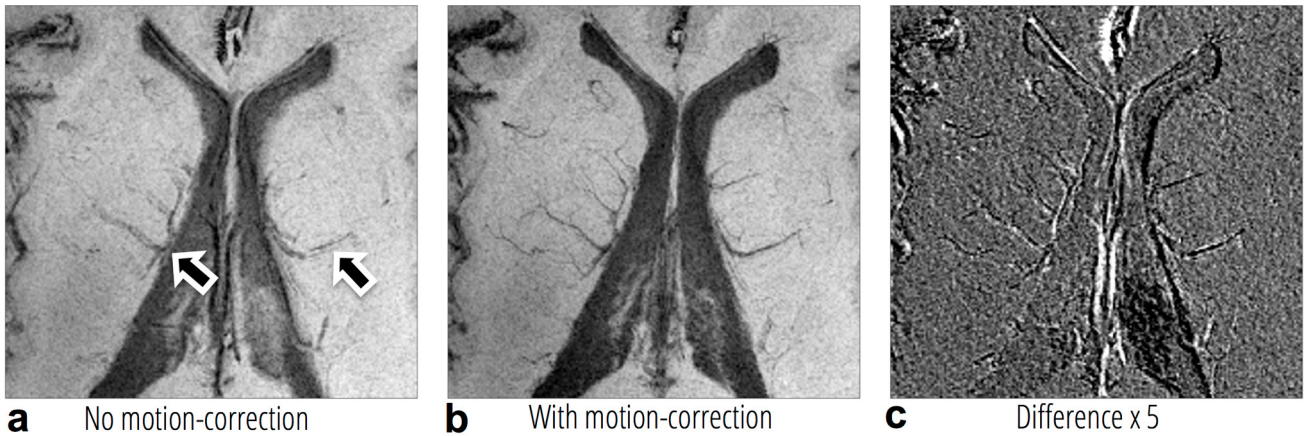
to become less well-defined, and increased noise and artifacts are visible. Even at the highest acceleration factor, however, the outline of the scalp remains recognizable.

Experiment 2: High-resolution MP2RAGE scan motion-corrected with 3D FatNavs

Figure 3a shows the rigid-body motion parameters estimated from the 3D FatNavs (2mm, 4×4 acceleration) during the ~37 minute MP2RAGE scan. All plots pass through zero at ~12 mins as this corresponds to the time of the acquisition of the center of k-space, and motion-parameters are defined relative to this head pose. The amplitude of the estimated motion is small, with a root-mean-square (RMS) displacement of 1.08 mm and RMS rotation of 0.84° during the ~37 minutes.

Figure 3b and Fig. 3c compare the MP2RAGE contrast, before and after motion-correction. When viewed at this scale the differences are nearly imperceptible. However, as illustrated by the difference image (Fig 3d), differences between the two are primarily high-resolution features.

The zoom of the MP2RAGE contrast shown in Fig. 4 demonstrates visible improvements in image quality

following motion-correction. This is mostly visible by comparing features with high spatial frequency information, such as arteries (bright), veins (dark in the white-matter towards the right of the image) and between the ventricles. Such high-resolution differences are confirmed by the difference image. Differences also become more obvious to the eye when the images are alternated as a movie – see Supporting Video S1 (available online).

It was found that visualizations of the blood vessels increase the visual perceptibility of the improvements in image quality following motion-correction. Figure 5 shows the minimum intensity projection over a 10 mm thick slab in the z-direction of a zoomed section of part of the GRE_{TI2} volume from the same MP2RAGE dataset. Visual inspection reveals noticeable improvements in vessel sharpness following motion-correction, and especially in the conspicuity of the smaller veins within the white-matter and deep-brain (see Supporting Video S2 online for a movie of the same image comparison).

Figure 6 shows a maximum intensity projection over the full 80 mm slab in the *z*-direction of the same GRE_{TI2}
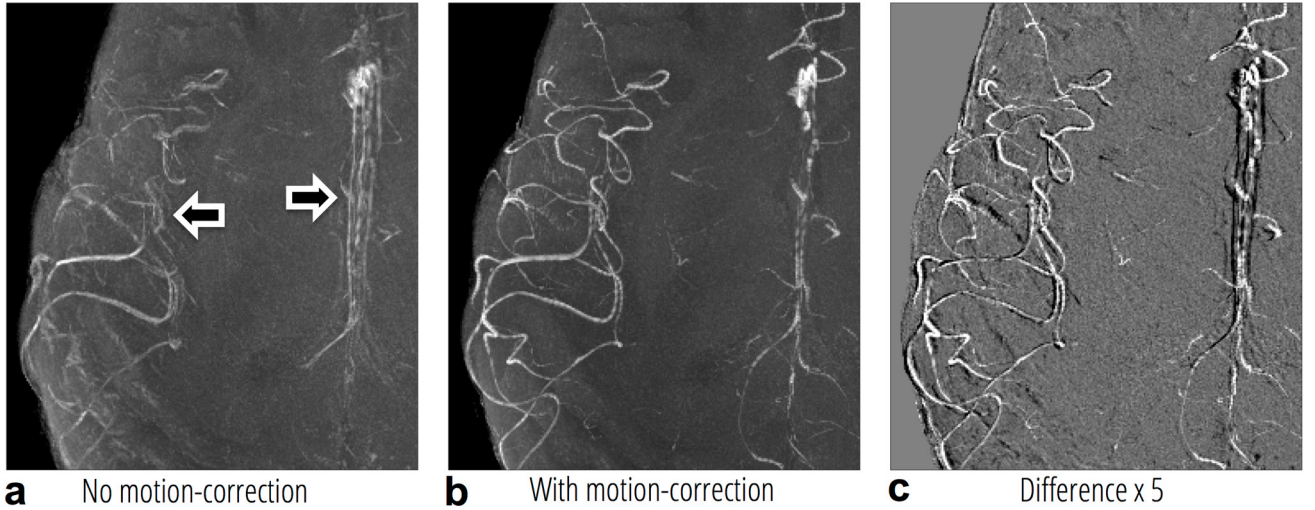
Figure 6. (a) A zoomed section of the GRE$_{TI2}$ volume from the same MP2RAGE dataset as shown in Figs. 3-5, with a maximum intensity projection taken over the full 80 mm slab in the z-direction. (b) The same section following retrospective motion-correction. (c) The difference between the two. The arrows in (a) indicate regions where the improvement is most prominent. The overall improvement is best appreciated from the animated version of this figure, viewable online as Supporting Video S3.

volume, visualizing the arteries. Again the main difference following motion-correction is an increased conspicuity of the smaller vessels (See Supporting Video S3 online for a movie of the same image comparison).

Experiment 3: High resolution TSE scan motion-corrected with 3D FatNavs

Figure 7a shows the estimated rigid-body motion parameters from the 3D FatNavs (2mm, 4×4 acceleration) during the ~34 minute TSE scan. The total motion for this subject was very small, with an RMS displacement of 0.40 mm and RMS rotation of 0.18°. All motion parameters pass through zero at around 17 mins, as all parameters have been shifted to coincide with the acquisition of the center of k-space.

Figures 7b and 7c compare orthogonal views of the whole high-resolution TSE dataset, before and after the application of retrospective motion-correction. While overall the images appear comparable, the difference image demonstrates that the major changes are high-spatial frequencies, i.e. edges (Fig. 7d).

When examining a zoomed sagittal view of the anterior of the brain from the same TSE dataset, clear improvements in delineation of image boundaries are observed, especially at the boundary between the very bright cerebrospinal fluid (CSF) and the grey matter (Fig. 8). Ringing artifacts across the cortex resulting from the bright CSF are also noticeably reduced following motion-correction. Larger arteries, which appear dark in these images, are also more clearly identifiable. An animated version of this figure is available online (Supporting Video S4).

Experiment 4: Detection of head-motion due to the respiratory cycle with FatNavs

Figure 9 shows the estimated motion parameters from the 2 minute scan consisting only of 3D FatNavs (4mm, 4×4 acceleration). Visual comparison shows that data from the respiratory belt explain much of the fluctuations observed in the estimated z-motion (Fig. 9c).

Discussion

Retrospective motion-correction

An advantage of the retrospective correction over prospective correction is that the uncorrected image is always also available. Even in the current proof-of-concept implementation with prolonged off-line processing of raw data, the original uncorrected images appear on the scanner via the standard reconstruction pipeline. In order for the method to be as robust as possible, it may be useful to devise an automated quality check of the corrected image to alert the user that they may wish to refer back to the original uncorrected images in the case of an anomaly in the retrospective pipeline.

In its current implementation, the retrospective motion-correction is limited to 3D sequences *without parallel acceleration*. Incorporation of support for parallel acceleration of the host sequence would require a reconstruction approach which is capable of dealing with k-space data which no longer conforms to a Cartesian grid, such as non-Cartesian SENSE (24). As this would present additional complications to implement robustly in 3D at high resolution, the results we present here were all acquired without parallel acceleration.

In principle, the 3D FatNav approach can also be used for *prospective* motion-correction, provided that real-time image reconstruction pipelines available on the scanner software/hardware and the available memory are capable of coping with the demands of highly accelerated GRAPPA (the computational load and memory-burden both increase with increasing acceleration factor). A more optimized approach to the image reconstruction would likely be required, both in terms of memory demands and processor-load, in order to reduce the latencies to an acceptable level for prospective motion-correction. The image co-registration also represents a significant computational burden, which would need to be optimized in this case.
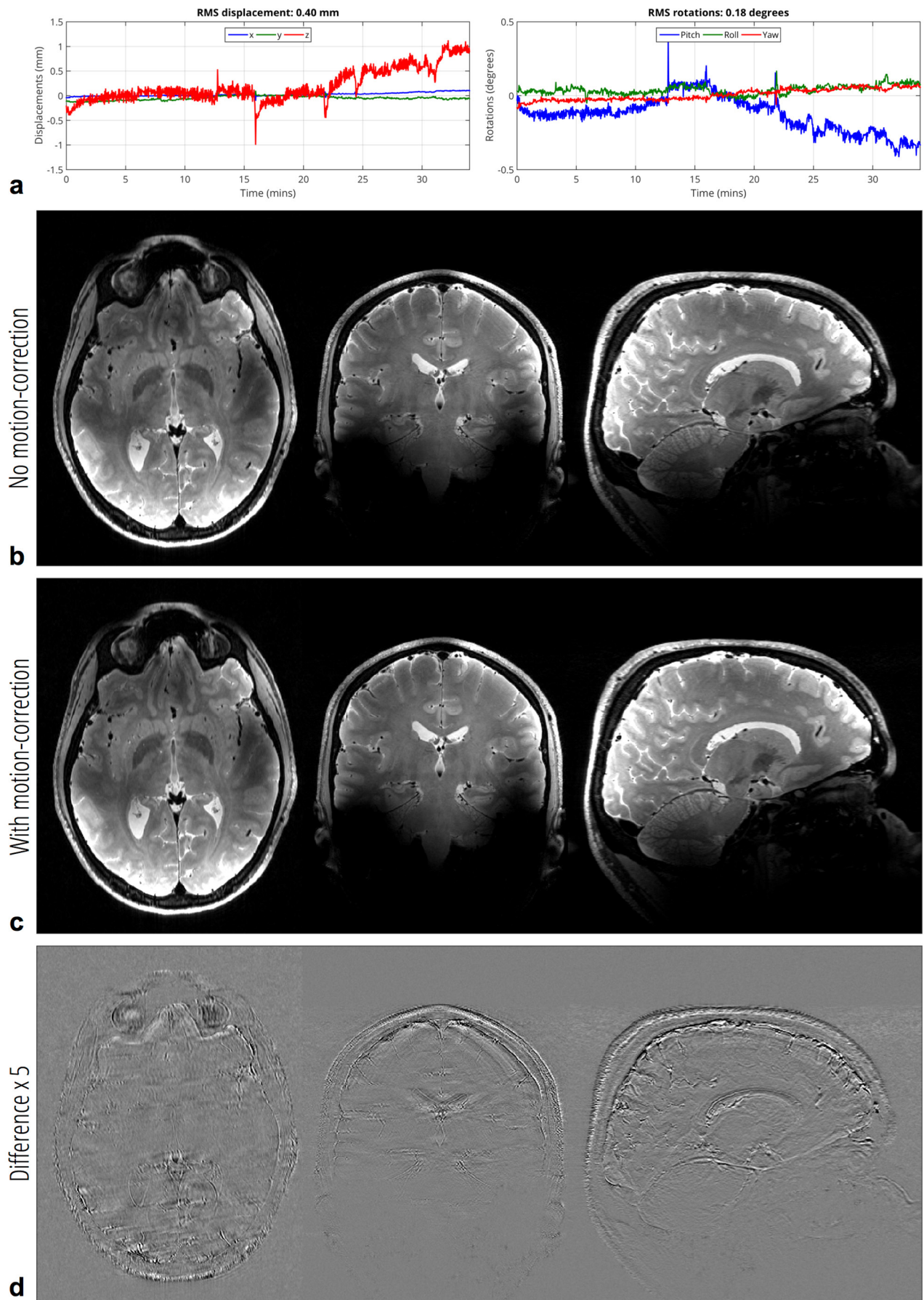
Figure 7. (a) Estimated rigid-body motion parameters obtained from 3D FatNavs (2mm, 4×4 acceleration) during ~34 minute TSE scan, 600 μm isotropic resolution (Experiment 3). (b) The high-resolution TSE volume. (c) The same TSE volume following retrospective motion-correction. (d) The difference between the two.
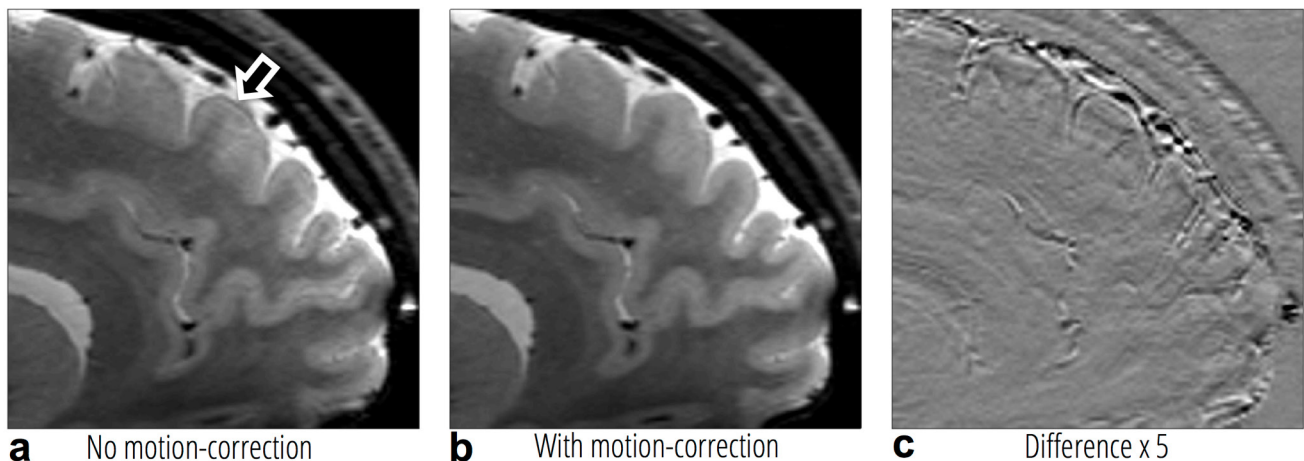
Figure 8. (a) Zoom of a sagittal view of the same TSE dataset as shown in Fig. 7. (b) The same zoom following retrospective motion-correction. (c) The difference between the two. The arrows in (a) indicate regions where the improvement is most prominent. The overall improvement is best appreciated from the animated version of this figure, viewable online as Supporting Video S4.

3D FatNav reconstruction and co-registration

For the chosen parameters of the 3D FatNavs (2mm, 4×4) used to estimate motion-parameters for the structural scans, we observe a high-precision of the motion estimates on the order of ~<25 μm and ~<0.025° (the estimated amplitude of the high-frequency fluctuations visible in Figs. 3a and 7a), but we do not have an independent measure of the remaining bias in these estimates. It is reassuring that the images from the host-sequence following motion-correction are visibly improved in terms of image sharpness – especially noticeable in the increased conspicuity of very small vessels. The current choices of resolution and acceleration for the 3D FatNavs are somewhat arbitrary – and further investigation will be necessary to determine the optimal parameters for a given dead-time available in a particular host sequence. This optimization, however, will inevitably also depend on both the choice of parallel imaging reconstruction method and the image registration parameters.

The results from Experiment 4 suggest that the even the lower-resolution 3D FatNavs (4mm, 4×4) are sufficiently sensitive to be able to track the small motion associated with the respiratory cycle – but in order to be able to usefully correct for this motion it becomes important to be able to usefully estimate the position in the respiratory cycle corresponding to when the host sequence data were acquired, rather than at the time of the navigator. As can be observed from Fig. 1, the timing of the MP2RAGE and TSE sequences is such that the chosen navigator used for those experiments would be too long to be able to correct respiratory-induced-movements. The quality of our preliminary results of motion-correction with FatNavs – where we do not expect to have corrected for respiratory-induced motion - suggests that correcting for the slow drifting movements over the entire scan duration is more critical to image quality than the faster oscillations due to the respiratory cycle. Further investigation is necessary to determine in which situations accurate correction of respiratory-induced motion might provide additional noticeable improvement in image quality.

Given that the fat signal is primarily localized to the tissue surrounding the skull, it is expected that there will be fewer identifiable structural features than in a typical brain image – which may impair convergence of the co-registration, especially in the case of rotations where the subject has a round head-shape. Our experience in a limited number of subjects is that the precision of motion-estimates is not prohibitively hindered by this effect, presumably as clear features such as the temporal muscle and the ocular fat surrounding the eyes (both visible in Fig. 2b) are able to help give robust co-registration. This assumption will need to be revisited after a greater number of subjects have been scanned.

For Experiment 3 there is noticeably more noise in the estimated z-displacement compared to the x and y displacements (Fig. 7a), an effect not observed in Experiment 2 (Fig. 3a). This is likely due to the difference in the respiration-induced motion between volunteers.

The co-registration of the 3D FatNavs was performed using SPM's *realign* tool – using the least-squares difference as the cost-function. This could potentially lead to biased motion estimates – especially if aliasing artifacts are present as a result of the high acceleration factors used. We expect that it could be beneficial to exploit the fact that a full 3D-image of the fat is generated from the GRAPPA calibration data acquired at the start of the acquisition. Each individual 3D FatNav is, to a first approximation, exactly the same image following some small rigid-body motion. Incorporating the prior knowledge of the object should allow improved reconstruction of each FatNav – and therefore more robust estimates of head motion.

We currently acquire the calibration data for the GRAPPA weights for the 3D FatNavs only once at the start of the scan (2.3s). If the subject motion is large, it may be beneficial to update the GRAPPA weights during the scan. This could be achieved without additional scan time if the k-space points acquired for each FatNav are shifted relative to the previous FatNav. As a consequence, for every 16 FatNavs acquired, a full coverage of k-space can be achieved (using 16-fold acceleration). It would also be possible in this way to have a 'sliding window' of GRAPPA
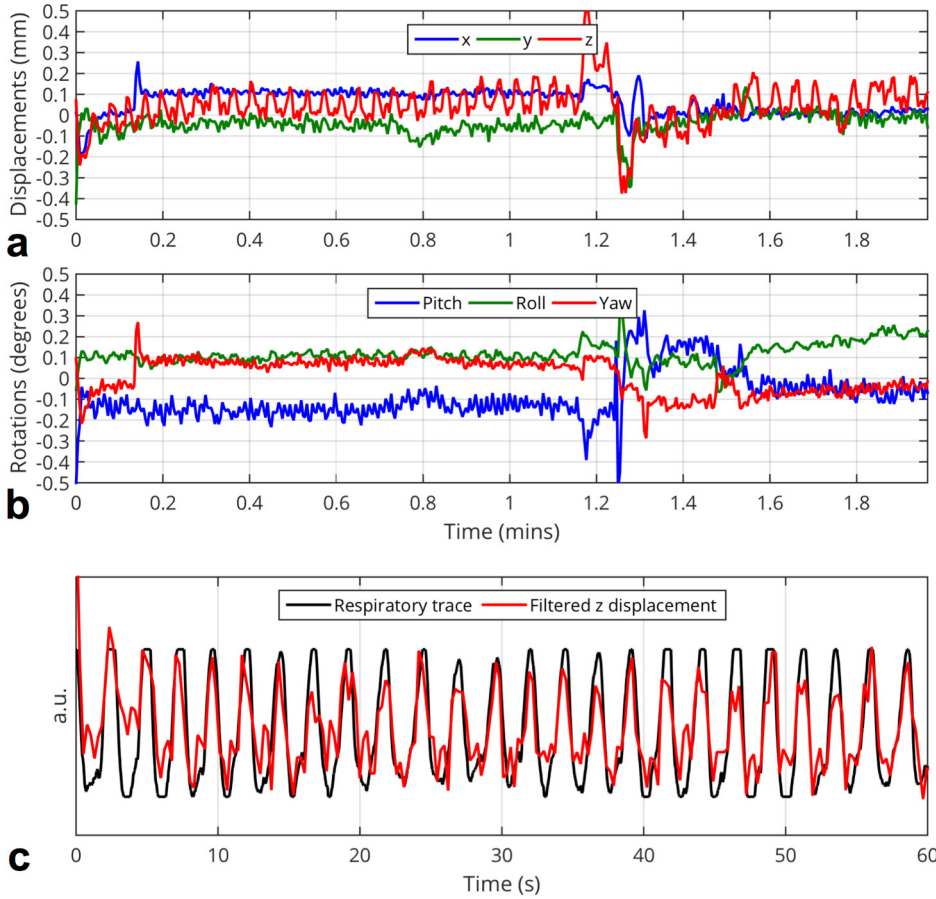
Figure 9. Estimated motion parameters from a 2-minute scan consisting only of 3D FatNavs, with resulting (a) translations and (b) rotations. (c) A zoom of the first 60 seconds of the estimated z-displacement (after high-pass filtering) shown on the same axes as the signal measured from a respiratory belt.

weights for the reconstruction of each individual FatNav to try to make the reconstruction more robust to aliasing artifacts by always having a set of GRAPPA weights from a head-pose as close as possible to the head-pose at the time of the FatNav. We primarily envisage early applications of the technique to remain with the correction of small involuntary motion of compliant subjects, however, as not only is larger motion more difficult to track accurately, but it will also lead to larger gaps in the corrected k-space of the host sequence, which can also lead to artifacts.

3D FatNavs at other field strengths
While the present study was conducted at 7T, the 3D FatNav is expected to be easily applied at lower fields. Although the duration of the binomial fat excitation will be longer due to the smaller frequency shift between fat and water resonances, this should not lead to prohibitively long scan times for the 3D FatNav.

3D FatNavs in other host sequences
We demonstrated the insertion of 3D FatNavs into an MP2RAGE and a TSE sequence, as these are both commonly used protocols which already have sufficient 'dead-time' to allow insertion of the navigator with no penalty in scan-time. It would also be desirable to be able to apply motion-correction to sequences such as high-resolution GRE for susceptibility-weighted imaging, but this will inevitably require a longer scan duration to incorporate the 3D FatNavs. There is therefore considerable interest in capturing high-resolution motion information in as short a navigator as possible. The remarkably high quality of the fat images presented in

Fig. 2 at exceptionally high acceleration factors might give the impression that acquisitions as short as 290 ms (8×8 acceleration) may still give high quality motion estimates. However, our preliminary results attempting to assess the increasing error and bias associated with increasing acceleration factor suggest that, at least with the current image registration pipeline, the (visually) small artifacts associated with the high acceleration factors can introduce unacceptable levels of bias in the motion estimates (25). Future work will investigate whether incorporating prior knowledge regarding the structure of these artifacts can improve motion-estimates from customized image registration algorithms for very fast FatNav acquisitions. Besides the increased scan duration, care will also need to be taken to ensure that FatNavs can be inserted without significantly disturbing the steady-state properties of the GRE host sequence, as has been successfully achieved for the EPI-based vNavs (26).

Conclusion
We have successfully demonstrated the feasibility of highly-accelerated fat-excitation volumes to be used as motion-navigators for the retrospective correction of microscopic involuntary movement of compliant subjects during high-resolution 3D structural scans of extended duration, yielding noticeable improvements in image quality even for very small motion of the subject.

References

1. Zaitsev M, Dold C, Sakas G, Hennig J, Speck O. Magnetic resonance imaging of freely moving objects: prospective real-time motion correction using an external optical motion tracking system. Neuroimage 2006;31:1038–50. doi: 10.1016/j.neuroimage.2006.01.039.

2. Ooi MB, Krueger S, Thomas WJ, Swaminathan S V, Brown TR. Prospective real-time correction for arbitrary head motion using active markers. Magn Reson Med 2009;62:943–54. doi: 10.1002/mrm.22082.

3. Schulz J, Siegert T, Reimer E, Labadie C, Maclaren J, Herbst M, Zaitsev M, Turner R. An embedded optical tracking system for motion-corrected magnetic resonance imaging at 7T. Magn Reson Mater Phy 2012;25:443–53. doi: 10.1007/s10334-012-0320-0.

4. Qin L, van Gelderen P, Derbyshire JA, Jin F, Lee J, de Zwart JA, Tao Y, Duyn JH. Prospective head-movement correction for high-resolution MRI using an in-bore optical tracking system. Magn Reson Med 2009;62:924–34. doi: 10.1002/mrm.22076.

5. Maclaren J, Armstrong BSR, Barrows RT, et al. Measurement and Correction of Microscopic Head Motion during Magnetic Resonance Imaging of the Brain. PLoS One 2012;7:e48088. doi: 10.1371/journal.pone.0048088.

6. Pipe JG. Motion correction with PROPELLER MRI: application to head motion and free-breathing cardiac imaging. Magn Reson Med 1999;42:963–9.

7. Anderson AG, Velikina J, Block W, Wieben O, Samsonov A. Adaptive retrospective correction of motion artifacts in cranial MRI with multicoil three-dimensional radial acquisitions. Magn Reson Med 2013;69:1094–103. doi: 10.1002/mrm.24348.

8. White N, Roddey C, Shankaranarayanan A, Han E, Rettmann D, Santos J, Kuperman J, Dale A. PROMO: Real-time prospective motion correction in MRI using image-based tracking. Magn Reson Med 2010;63:91–105. doi: 10.1002/mrm.22176.

9. Van der Kouwe AJW, Benner T, Dale AM. Real-time rigid body motion correction and shimming using cloverleaf navigators. Magn Reson Med 2006;56:1019–32. doi: 10.1002/mrm.21038.

10. Welch E, Manduca A. Spherical navigator echoes for full 3D rigid body motion measurement in MRI. Magn Reson Med 2001;41:32–41. doi: 10.1002/mrm.10012.

11. Tisdall MD, Hess AT, Reuter M, Meintjes EM, Fischl B, van der Kouwe AJW. Volumetric navigators for prospective motion correction and selective reacquisition in neuroanatomical MRI. Magn Reson Med 2012;68:389–99. doi: 10.1002/mrm.23228.

12. Schulze P, Stucht D, Danishad KA, Kadashevich IY, Herbst M, Lovell-smith C, Maclaren J, Barrows RT, Kusik TP. Prospective motion correction to increase the achievable resolution in brain imaging at 7T. Proc. 20th Annu. Meet. Int. Soc. Magn. Reson. Med. Melbourne, Aust. 2012:597.

13. Tisdall MD, Polimeni JR, van der Kouwe AJW. Motion-corrected 350 μm isotropic MPRAGE at 3 T using volumetric navigators (vNavs). In: Proceedings of the 21st Annual Meeting of the International Society of Magnetic Resonance in Medicine, Salt Lake City, USA. Vol. 33. ; 2013. p. 268.

14. Nguyen TD, Nuval A, Mulukutla S, Wang Y. Direct monitoring of coronary artery motion with cardiac fat navigator echoes. Magn Reson Med 2003;50:235–41. doi: 10.1002/mrm.10550.

15. Van der Kouwe AJW, Benner T, Wald LL. Decoupling motion navigation from imaging using spatial-spectral RF pulses. In: Proceedings of the 16th Meeting of the International Society for Magnetic Resonance in Medicine, Toronto. ; 2008. p. 1465.

16. Skare S, Hartwig A, Mårtensson M, Avventi E, Engström M. Properties of a 2D fat navigator for prospective image domain correction of nodding motion in brain MRI. Magn Reson Med (Early View online) 2014;00:1–10. doi: 10.1002/mrm.25234.

17. Griswold MA, Jakob PM, Heidemann RM, Nittka M, Jellus V, Wang J, Kiefer B, Haase A. Generalized autocalibrating partially parallel acquisitions (GRAPPA). Magn Reson Med 2002;47:1202–1210. doi: 10.1002/mrm.10171.

18. Gallichan D, Marques JP, Gruetter R. Overproof GRAPPA: Exploiting natural sparsity of fat images for 64-times accelerated motion navigators (FatNavs). In: Proceedings of the 22nd Annual Meeting of the International Society of Magnetic Resonance in Medicine, Milan, Italy. ; 2014. p. 4345.

19. Marques JP, Kober T, Krueger G, van der Zwaag W, Van de Moortele P-F, Gruetter R. MP2RAGE, a self bias-field corrected sequence for improved segmentation and T1-mapping at high field. Neuroimage 2010;49:1271–81. doi: 10.1016/j.neuroimage.2009.10.002.

20. Fessler J, Sutton B. Nonuniform fast Fourier transforms using min-max interpolation. IEEE Trans. Signal Process. 2003;51:560–574.

21. Van de Moortele P-F, Auerbach EJ, Olman C, Yacoub E, Uğurbil K, Moeller S. T1 weighted brain images at 7 Tesla unbiased for Proton Density, T2* contrast and RF coil receive B1 sensitivity with simultaneous vessel visualization. Neuroimage 2009;46:432–46. doi: 10.1016/j.neuroimage.2009.02.009.

22. Zhang Y, Brady M, Smith S. Segmentation of brain MR images through a hidden Markov random field model and the expectation-maximization algorithm. IEEE Trans. Med. Imaging 2001;20:45–57. doi: 10.1109/42.906424.

23. Mugler J, Kiefer B, Brookeman J. Three-Dimensional T2-Weighted Imaging of the Brain Using Very Long Spin-Echo Trains. In: Proceedings of the 8th Annual Meeting of the International Society for Magnetic Resonance in Medicine, Dever, CO. ; 2000. p. 687.

24. Pruessmann KP, Weiger M, Börnert P, Boesiger P. Advances in sensitivity encoding with arbitrary k-space trajectories. Magn Reson Med 2001;46:638–51.

25. Gallichan D, Marques JP, Gruetter R. Optimizing a highly-accelerated FatNav for high-resolution motion-correction. In: Proceedings of the 23rd Annual Meeting of the ISMRM, Toronto, Canada. ; 2015. p. (submitted).

26. Tisdall MD, Bhat H, Heberlein K, van der Kouwe AJW. Prospective head motion correction in 3D FLASH using EPI-based volumetric navigators (vNavs). In: Proceedings of the 22nd Annual Meeting of the International Society of Magnetic Resonance in Medicine, Milan, Italy. Vol. 67. ; 2014. p. 882.